Microfluid Nanofluid (2006) 2: 367–379
DOI 10.1007/s10404-006-0087-6

REVIEW

**Ralf Zimmermann · Toshihisa Osaki**
**Rüdiger Schweiß · Carsten Werner**

# Electrokinetic microslit experiments to analyse the charge formation at solid/liquid interfaces

Received: 20 January 2006 / Accepted: 17 February 2006 / Published online: 18 March 2006


**Abstract** Electrokinetic effects play an important role in microfluidics and nanofluidics. Although the related phenomena are often utilized to control fluid flow and sample transport in lab-on-a-chip devices, their dependency on the surface charges on the channel walls often remain enigmatic. This is mainly due to the lack of adequate experimental methods to analyse the electrical charging of solid/liquid interfaces of interest. To address this need, an experimental set-up—designated as microslit electrokinetic set-up (MES)—has been recently developed and applied for the investigation of charge formation processes at planar solid/liquid interfaces. The device permits to perform streaming potential and streaming current measurements across a rectangular streaming channel formed by two parallel sample carriers (20×10×3 $mm^3$) at variable distance allowing for the determination of the surface conductivity. Utilizing the MES, charge characteristics can be determined for a wide variety of materials prepared as thin films on top of planar glass substrates. Streaming potential and streaming current data permit to investigate the mechanisms of charge formation while surface conductivity data provide information about mobile charge carriers located in different zones at the interface. The applicability of this advanced experimental approach is demonstrated with examples obtained for surfaces with different levels of complexity:

1. Preferential ion adsorption onto unpolar fluoropolymer (Teflon® AF) films was characterized in simple electrolyte solutions; the results were quantitatively evaluated with respect to interfacial ion concentrations.
2. Interrelation of charge density and conformation of grafted poly(L-glutamic acid layers) were unravelled from the determination of pH-depended variations of surface conductivity and layer thickness.
3. The impact of spatial confinements of surface functional groups on their acid–base behaviour was studied with self-assembled monomolecular films of alkanethiols chemisorbed on gold.
4. Charging of and ion mobility within poly(acrylic acid) (PAA) brushes prepared by a Langmuir–Blodgett technique were analysed at varied pH and ionic strength.
5. Interfacial modes of adsorbed proteins were distinguished at two polymer surfaces with varied hydrophobicity/charge density.

**Keywords** Zeta potential · Surface conductivity · Microslit · Polymer · Surface charge

R. Zimmermann · T. Osaki · C. Werner (✉)
Leibniz Institute of Polymer Research Dresden,
Max Bergmann Center of Biomaterials Dresden,
Hohe Strasse 6, 01069, Dresden,, Germany
E-mail: werner@ipfdd.de
Tel.: +49-351-4658532
Fax: +49-351-4658533

R. Schweiß
Institute of Materials Research and Engineering,
3 Research Link, Singapore, 117602, Singapore

C. Werner
Department of Mechanical and Industrial Engineering,
University of Toronto, 5 King's College Road, Toronto,
ON, Canada, M5S 3G8

## 1 Introduction

In many applications, solid surfaces contact aqueous media (Riepl et al. 1999; Fodor et al. 1993; Jeon and Andrade 1991; Uyama et al. 1998). The resulting formation of an interfacial electric charge often determines the characteristics of the solid/liquid interface. Interfacial charge was found to be relevant for a number of fundamental phenomena such as wetting, adsorption and adhesion (Grundke et al. 1995; Bismarck et al. 1999; Schmitt 2002) and, thus, crucial for a wide variety of technologies. The kinetics of conjugation between ligands (proteins and nucleic acids) and biosensor surfaces (Liu et al. 2000; Baerga-Ortiz et al. 2000) as well as

transport and separation processes in microscale bioanalytic devices (Erickson and Li 2002; Stroock et al. 2000) depend on the charge at the interface, and on the electrokinetic and electrodynamic phenomena associated with this charge. Therefore, the comprehensive characterization of electrosurface phenomena at nonconducting solid materials adjacent to aqueous solutions is an important but not yet sufficiently addressed task in the rational design of lab-on-a-chip systems. Importantly, the experimental assessment of surface charge is required to permit the rational design of the surface chemistry and structure on the channel walls of microfluidic systems to enhance the electroosmotic transport of fluids and the electrophoretic separation of samples in lab-on-a-chip devices and to direct electrostatic interactions between proteins and the microfluidic channels.

Potentialities and limitations of the experimental assessment of electrosurface phenomena are very often related to the determination and interpretation of the zeta potential. This quantity is defined as the potential 'at the plane of shear'—an imaginary plane separating the solution adjacent to a smooth and charged interface into two zones: an inner region where no fluid motion occurs (hydrodynamic immobile layer) and an outer region where fluid velocity takes non-zero values (Lyklema 1995). Zeta potentials are derived from the analysis of electrokinetic effects which, briefly, consist of the tangential displacement of a solid phase and an aqueous solution caused by an external electrical field, or inversely, consist of a charge separation by an external mechanical force acting on the system to tangentially shift the two phases. Electrokinetic measurements were found to be a valuable tool providing direct information on the charge of solid/liquid interfaces (Hunter 1981). This marks a major advantage of this method when compared with experiments rather indirectly related to the interfacial charge (Garbassi et al. 1996). Since the electrokinetic experiment considers the compensation of surface charge by the ions of the double layer on the liquid side of the interface it is often very useful when investigating problems of practical relevance (Jacobasch 1984; Werner et al. 1999). Electrokinetic measurements are—as another advantage—applicable to solids of different shapes which has stimulated the development of a variety of instruments for the electrokinetic characterization of particles/dispersions and macroscopic solid samples (van der Put 1980; Nitzsche and Simon 1997; van Wagenen and Andrade 1980; Jacobasch and Schurz 1988).

However, very often the interpretation of electrokinetic measurements is not unambiguous due to the presence of physicochemical heterogeneity of the surface, i.e. roughness, porosity, hairy layers or a patch-like distribution of chemical properties. This fact was experienced as an apparent lack of reliability in several experimental approaches but also provoked efforts to extend both electrokinetic experiments and theory (Lyklema and Rovillard 1998; Ohshima 1995; Werner et al. 1998; Duval and van Leeuven 2004; Yezek 2005; Dukhin et al. 2004, 2005). As an important conclusion to be drawn from these activities for a majority of relevant samples additional information about the analysed interface is required for any reasonable interpretation of electrokinetic experiments.

The surface conductivity $K^{\sigma}$ (also designated as specific surface conductivity or interfacial conductivity) can be considered as a very valuable parameter for that aim since it independently reflects the ion accumulation at the solid/liquid interface. In the context to be discussed here, surface conductivity represents an excess conductivity of the interface due to the accumulation of ions within the electrical double layer. Usually, surface conductivity is treated in projection on an assumed interfacial plane according Eq. 1:

$$K^{\sigma} = F \sum_i |z_i| \int_0^{\infty} [c_i(x) - c_i(\infty)]\, u_i(x)\, \mathrm{d}x, \tag{1}$$

where $F$ is the Faraday constant, $i$, the index of different ionic species, $z$, the valency of the ions, $c(x)$, the ion concentration perpendicular to the surface, $c(\infty)$, the ion concentration of the bulk solution, $u$, the mobility of the ions and, $x$, the distance from the surface.

As an important advantage, surface conductivity is not related to any hydrodynamic slipping process and, thus, not affected by properties influencing the liquid flow at the interface. Although the resulting potentialities were pointed out by Dukhin (Dukhin and Derjaguin 1974) and a few others already, many years ago many authors continued to treat surface conductivity rather as an unspecified correction term for zeta potential calculations from experimental data. However, the value of surface conductivity data and the contained information was recognized by a wider range of scientists in the last few years (Werner et al. 1998; Löbbus et al. 2000; Minor et al. 1998; Zimmermann et al. 2003).

Starting from the work of Bikerman (1935) the presence of mobile ions in the diffuse part of the electrical double layer was for a long period, the only discussed origin of the occurrence of surface conductivity. However, recently the contribution of conductivity "behind" the slipping plane was found to be a substantial share of the total surface conductivity in several cases (Werner et al. 1998; Löbbus et al. 2000; Minor et al. 1998; Zimmermann et al. 2003). This effect will be emphasized referring to several examples in Sect. 4 of this article. For hydrophilic or conducting solid materials even the volume phase of the solid may give rise to this type of conductivity to a considerable extent.

Encouraged by the fundamental work and personal advice of Stanislav S. Dukhin the authors of this article designed, built and applied a new device for the determination of the surface conductivity from streaming potential and streaming current measurements across rectangular slit channels formed between two planar samples. The set-up can be applied for the characterization of electrosurface phenomena at a wide variety of materials prepared as thin films on top of planar,

macroscopic glass carriers. The dimensions of those carriers easily permit the comprehensive surface characterization of the analysed materials by surface spectroscopies, microscopies and optical thickness measurements at similar samples. Subsequently, the microslit electrokinetic set-up (MES) will be briefly introduced. In addition, examples for the analysis of interfacial charge at thin organic films in aqueous solutions by means of the MES will be reported to demonstrate its versatile applicability.

## 2 Design and operation of the microslit electrokinetic set-up

The MES is an in-house-built instrument for the electrosurface characterization of planar samples. It permits the perform streaming potential and streaming current measurements at a rectangular streaming channel formed by two parallel sample carriers (Fig. 1, Körber et al. 1999). As a key feature of the device the distance between the sample surfaces can be adjusted down to 1 μm keeping the surfaces parallel and without de-wetting of the samples.

A cross-section of the sample carrier and positioning unit is shown in Fig. 2. Polymer-coated sample carriers are fixed on a glass block and aligned in parallel under microscope. After the alignment, the slit formed by the sample carriers is sealed by silicon gaskets from all four directions simultaneously by a pneumatic system. Ag/AgCl electrodes for the measurement of the streaming potential and streaming current are positioned at the inlet and outlet of the channel. The precise distance adjustment is performed by means of a piezotranslator.

Streaming potential and streaming current measurements can be performed with the MES at varied pressure differences across the slit channel automatically including variation of electrolyte, its concentration and pH plus variation of the channel height, respectively.

Provided that the conditions for "standard electrokinetic substrates" to be fulfilled, i.e. the sample exhibits a molecular smooth, non-porous and chemical homogeneous surface, the zeta potential, $\zeta$, can be derived from the streaming potential, $U_S$, and streaming current, $I_S$, data based on the Smoluchowski equations:

$$\zeta(U_S) = \frac{\eta K_B}{\varepsilon_0 \varepsilon_r} \frac{dU_S}{dp}\bigg|_{Du \ll 1}, \tag{2}$$

$$\zeta(I_S) = \frac{\eta L}{\varepsilon_0 \varepsilon_r bh} \frac{dI_S}{dp}, \tag{3}$$

where $\eta$ is the dynamic viscosity of the fluid, $K_B$, the specific electrical conductivity of the fluid, $\varepsilon_0$, the permittivity of vacuum, $\varepsilon_r$, the dielectric constant of the fluid and, $p$, the pressure difference across the slit channel. The conditions for the applicability of Eq. 2 are given by the Dukhin number Du (Lyklema 1995). For rectangular streaming channels Du is defined by the dimensionless ratio $K^{\sigma}/hK_B$, i.e. Eq. 2 can be used for the evaluation of the streaming potential measurements at high electrolyte concentrations and large channel heights.

The fluid flow $Q$ measured at several pressure differences $p$ permits to determine the slit channel height $h$:

$$h = \sqrt{[3]}\frac{12\eta L}{b}\frac{1}{n}\sum_{i=1}^{n}\frac{Q_i}{p_i}. \tag{4}$$

Independent of the flow measurements, the determination of a reference channel height $h_0$ can be based on streaming current measurements ($dI_S/dp$) at different channel heights $h_i$ ($h_i = h_0 + \Delta h_i$). Substituting $h$ in Eq. 3 by $h_0 + \Delta h_i$ one obtains

$$\frac{\eta L}{\varepsilon_0 \varepsilon_r b}\left(\frac{dI_S}{dp}\right)_i = \zeta \Delta h_i + \zeta h_0. \tag{5}$$

Using this expression (5), $h_0$ can be derived by a linear regression.

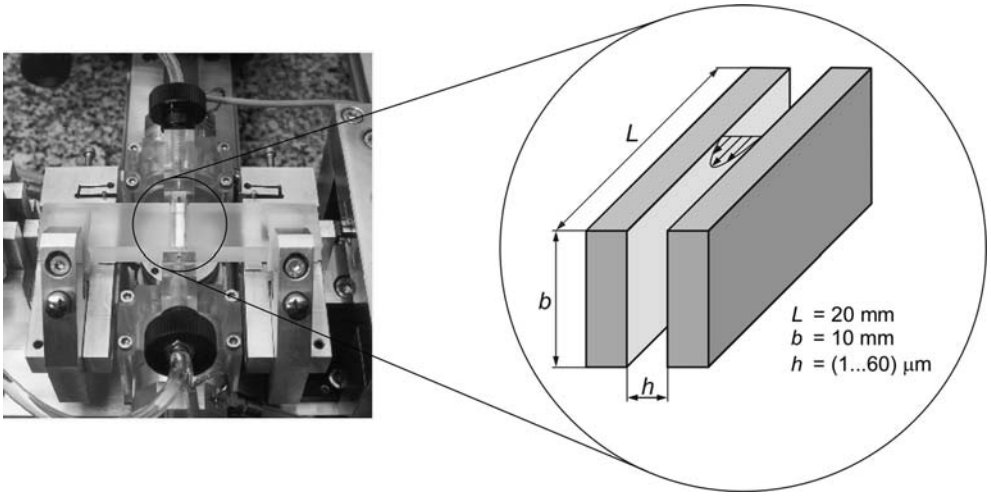


**Fig. 1** Microslit cell after alignment of the sample carriers (left) and schematic representation of the streaming channel (right)

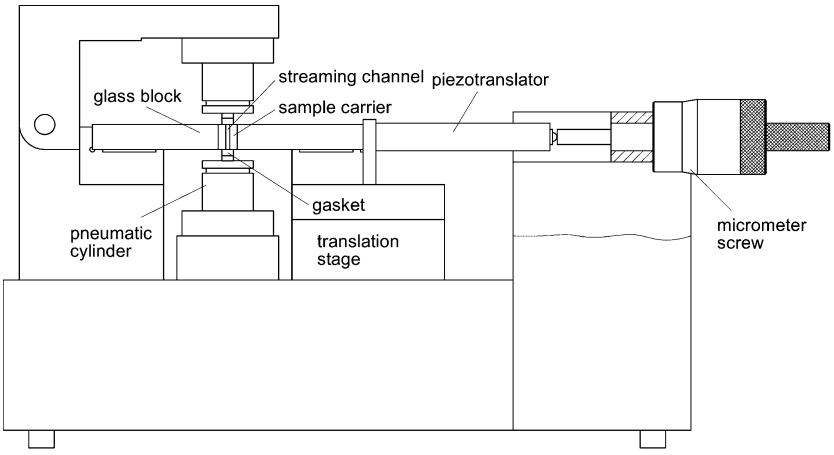


**Fig. 2** Microslit electrokinetic set-up: cross-section of the sample carrier and positioning unit

The streaming potential and streaming current values obtained for a number of sufficient small channel heights $h$ are used to calculate the surface conductivity $K^{\sigma}$ according to Eq. 6:

$$\frac{\mathrm{d}I_S/\mathrm{d}p}{\mathrm{d}U_S/\mathrm{d}p}\frac{L}{2b} = \frac{K_B}{2}h + K^{\sigma}. \qquad (6)$$

## 3 Materials

Samples for MES experiments summarized in this work had been prepared according to the following procedures:

1. *Teflon® AF films* were obtained by spin-coating of polymer solutions purchased from DuPont, Neymours, US onto glass or Si wafer using a commercial spin-coater (Karl Suss, Saint Jeoire, France). By adjustment of the solution concentration (2% AF1601 in FC75) and velocity of the coater disk smooth and homogeneous films were obtained. The polymer films were vacuum-dried and tempered 1 h at 165°C. The layer thickness of the Teflon® AF films layer has been determined to (118 ± 5) nm by variable angle spectroscopic ellipsometry (M44, Woolam Co., Lincoln, NE, USA). Dynamic water contact angles—measured by means of axisymmetric drop shape analysis (ADSA, developed by Prof. A.W. Neumann, University of Toronto, Department of Mechanical and Industrial Engineering) revealed the Teflon® AF layer to be very hydrophobic ($\theta_{adv} = 121°$, $\theta_{rec} = 112°$). The morphology of the polymer layer has been characterized by AFM (Bioscope, Digital Instruments, Santa Barbara, USA). The determined degree of roughness is in the range of few nanometers ($R_a = 0.2, \ldots, 0.8$ nm). The elemental composition of the polymer surface (F:O:C = 57:11:32) was determined by X-ray-photoelectron spectroscopy (ESCA-Lab 2, Vision Instruments, UK) to exclude dissociating surface groups.

2. *Grafted poly* (L-*glutamic acid*) *films* were produced by a surface initiated polymerization process. First, the surface of the glass carriers was modified with amino groups by immersing into a 1% solution of aminopropyltriethoxysilane (Aldrich) in ethanol. After 60 min, the substrates were removed form the solution, rinsed with ethanol and heated for 60 min at 100°C. This amine modified surface is used as an initiator layer for the surface induced polymerization.

To obtain the poly(L-glutamic acid) layers, the modified substrates are reacted with a solution of the *N*-carboxyanhydride of $\gamma$-*t*-butyl-L-glutamate in tetrahydrofuran. After 24 h, the substrates were rinsed with tetrahydrofuran and treated with formic acid in order to remove the *t*-butyl protecting groups. After 18 h, the substrates were removed and rinsed with de-ionized water.

3. *Self-assembled monolayers* (SAMs) on gold were prepared by overnight deposition from solutions of 11-mercapto-1-undecanol (MUD, Aldrich), 11-mercaptoundecanoic acid (MUA, Aldrich), 16-mercaptohexadecanoic acid (MHA, Aldrich) and hexadecanethiol (HDT) with an overall thiol concentration of 0.2 mM. For self-assembly of one-component monolayers and MUD/MUA mixtures absolute ethanol was used, whereas MHA/HDT mixtures were deposited from THF (anhydrous) solutions. Gold substrates were prepared by subsequent thermal evaporation (Leybold Univex) of 2 nm chromium and 150 nm gold onto borofloat glass slides. Thereafter, the gold surfaces were treated in a plasma cleaner (Harrick) and instantaneously immersed in the thiol solutions.

After assembly, the samples were removed from the thiol solution, rinsed thoroughly with absolute ethanol and blown dry in a stream of argon. Surface analysis of these monolayers using contact angle measurements, XPS, FTIR, AFM and ellipsometry has been reported recently (Schweiss et al. 2004). In particular, surface characterization of mixed monolayers by X-ray photoelectron spectroscopy showed good correlation of the surface composition and the mole fractions of the deposition solution for the mixed monolayers prepared based on this protocol. Tapping mode AFM measurements with hydrophilic/hydrophobic tips further indicated that for

the binary system MHA/HDT no phase separation exceeding the lateral resolution of this method could be observed. Therefore, even the polar–unpolar mixtures like MHA/HDT can be considered as homogeneous at least above the molecular level.

4. *Poly* (*acrylic acid*) *brushes* were prepared by means of a Langmuir–Blodgett method described by Currie et al. (1999b, c, d, 2000). In short, monolayers of a $(PS)_{34}-(PAA)_{368}$ block-copolymer at an air/water interface were prepared in a Langmuir trough, and pressure-area isotherms were determined. At an interfacial area of 10 $nm^2$ per polymer molecule PS-coated glass carriers were dipped (air → water) and retracted (water → air) through the $(PS)_{34}-(PAA)_{368}$ monolayers at a speed of 1 $mm^2/s$, while keeping the interfacial pressure and, hence, the area per polymer molecule in the monolayer constant. Thus, a single layer of $(PS)_{34}-(PAA)_{368}$ was transferred from the monolayer at the air/water interface onto PS-coated carriers. Usually, a transfer ratio of unity was achieved, resulting in a polymer grafting density at the carrier that is the same as the one selected at the air/water interface, i.e. 10 $nm^2$ per polymer chain. The samples were dried and heated for 5 min at 95°C (which is just beyond the glass temperature of PS); this treatment ensures that the PS block of the copolymer fuses with the PS coating and is essentially irreversibly attached after cooling to room temperature. Continuous washing with water did not remove any $(PS)_{34}-(PAA)_{368}$ from the surface, as probed by optical reflectometry under flowing water. Thus, the PS indeed firmly 'anchors' the $(PAA)_{368}$ chains on the surface. It has been ascertained that at the chosen grafted chain density of 0.1 $nm^{-2}$ the $(PAA)_{368}$-layers adopt a brush conformation (Currie et al. 1999a).

5. *Thin films of poly* (*octadecene-alt-maleic acid*) (POMA, Polysciences Inc., Warrington, PA) and *poly* (*propene-alt-maleic acid*) (PPMA, Leuna-Werke AG, Germany) were prepared on top of the glass carriers as follows (Pompe et al. 2003; Osaki and Werner 2003): anhydride POMA and PPMA were dissolved in tetrahydrofuran (0.08 wt.%) and methylethylketone (0.1 wt.%), respectively, spin-coated on the substrates which were modified with 3-aminopropyldimethylethoxysilane (ABCR GmbH& Co. KG, Germany) immediately after cleaned with mixture of ammonium hydroxide and hydrogen peroxide solution, and annealed at 120°C for 2 h to form stable imide bonds to the substrates. The rest of anhydride moieties were subsequently hydrolysed by autoclaving prior to the adsorption experiments. Physicochemical properties of the films were demonstrated elsewhere (Pompe et al. 2003, 2005; Osaki and Werner 2003). In this study, the density of covalent anchorages regarding the silane modification was adjusted to obtain the similar isoelectric points between POMA and PPMA films although the estimated charge densities from XPS data (Pompe et al. 2003) were different.

All solutions for electrokinetic measurements were prepared from de-ionized water, which has been vacuum-degased prior use. The electrolyte concentrations have been obtained by the addition of 0.1 M KCl, 0.1 M KOH or 0.1 M HCl solution.

Fibronectin (FN) solution was purified from adult human plasma following the protocol of Brew and Ingham (1994).

## 4 Results and discussion

### 4.1 Charge formation by unsymmetrical ion adsorption

To unravel details of the charge formation process of unsymmetrical ion adsorption Teflon® AF films were used as a model polymer substrate without any dissociable functionalities. It was known from several earlier studies that in those cases preferential adsorption of simple electrolyte ions may lead to rather high zeta potential values (Jacobasch 1984; Werner et al. 1999). By the determination of the zeta potential in dependence of the KOH, HCl and KCl solution concentration, the impact of the different dissolved ions on the formation of surface charge at the apolar polymer surface became evident (Fig. 3): The strongest preferential adsorption was observed for the hydroxide ions which predominate over the adsorption of the hydronium ions. No effect of preferential adsorption was found for the $K^+$ and $Cl^-$ ions (Zimmermann et al. 2001).

For several compositions of the electrolyte solution the surface conductivity was determined based on the variation of the channel geometry. Results of the quantification of zeta potential and surface conductivity for Teflon® AF in several solutions are given in Fig. 3.

For the given ideally smooth and homogeneous solid surface without dissociating surface sites, we may conclude from the charge density of the diffuse layer ($\sigma_d$) on the excess charge density of the inner layer ($\sigma_{i,e}$):

$$\sigma_{i,e} = -\sigma_d, \tag{7}$$

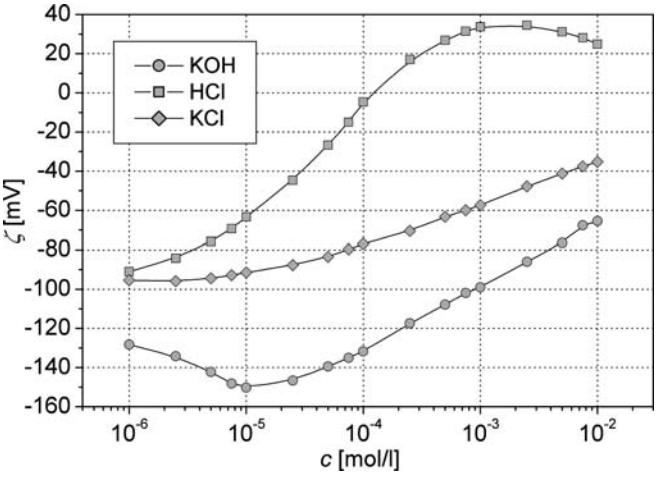


**Fig. 3** Zeta potential of Teflon® AF in dependence of the KOH, HCl, and KCl solution concentration

where $\sigma_d$ can be obtained from the experimentally determined zeta potential and the solution concentration:

$$\sigma_d = \sqrt{8\varepsilon_0\varepsilon_r RTc}\sinh\left(\frac{zF\zeta}{2RT}\right). \quad (8)$$

Corresponding to the charge density $\sigma_d$, the conductivity of the diffuse layer can be calculated according to

$$K^{\sigma,d} = \frac{2z^2F^2c}{RT\kappa}\left[D_+\left(e^{-zF\zeta/2RT}-1\right)\left(1+\frac{3m_+}{z^2}\right) + D_-\left(e^{zF\zeta/2RT}-1\right)\left(1+\frac{3m_-}{z^2}\right)\right], \quad (9)$$

where $m_\pm = (RT/F)^2(2\varepsilon_0\varepsilon\, r/3\eta D\pm)$ describes the relative contribution of the electroosmosis to $K^{\sigma,d}$ and $\kappa^{-1}$ is the Debye radius (Bikerman 1935). Equation 9 involves the assumption that $\zeta$ and $\Psi_d$ coincide. If this prerequisite is fulfilled the calculation provides precise results since the composition of the bulk electrolyte phase is known and the ion concentration in the diffuse layer is simply attributed to electrostatics. If the diffuse layer conductivity ($K^{\sigma,d}$) is known the inner layer conductivity $K^{\sigma,i}$ is obtained from the experimentally determined data of $K^\sigma$ to Eq. 10:

$$K^{\sigma,i} = K^\sigma - K^{\sigma,d}. \quad (10)$$

The inner layer conductivity expected for the excess of the charge determining ions ($K_e^{\sigma,\,i}$) can be estimated by Eq. 11 using the bulk mobilities which might be considered as upper boundaries of the probable range:

$$K_e^{\sigma,i} = |\sigma_{i,e}|u_{i,e}, \quad (11)$$

where $u_{i,e}$ is the mobility of the potential determining ion. The corresponding surface concentration $\Gamma_e$ of the excess charge carriers can be obtained by Eq. 12:

$$\Gamma_e = \frac{1}{F}\frac{|\sigma_{i,e}|}{|z|}. \quad (12)$$

The difference between $K^{\sigma,\,i}$ and $K^{\sigma,\,i}_e$ can be evaluated according to Eq. 13 to estimate the surface concentration $\Gamma_n$ of cations and anions in the inner layer which neutralize each other and therefore do not contribute to the surface charge:

$$\Gamma_n = \frac{K^{\sigma,i} - K_e^{\sigma,i}}{|z|F(u_+ + u_-)}. \quad (13)$$

The sum of the excess ion concentration and the surface concentration of anions and cations which neutralize each other provides the total ion concentration in the inner layer, which can be converted to the values for the areas $A_I$ per inner layer ion:

$$A_I = \frac{1}{N_A(\Gamma_e + \Gamma_n)}. \quad (14)$$

The results of this evaluation are given in Table 1. The presented data are unique by indicating the content of neutralized ions in the inner layer and, thus, the total density of ions in the stagnant part of the interface. It is evident that despite of the rather high zeta potential values obtained the ion density in the inner layer remains far below monolayer coverage. There is an increase of the inner layer ion density with increasing ionic strength of the electrolyte solution and with their content of charge determining ions.

**Table 1** Experimentally determined values of $\zeta$, $K^\sigma$, $\Gamma_e$, $\Gamma_n$, and $A_I$ for Teflon® AF in different electrolyte solutions

| Solution | $\zeta$ ($I_S$) (mV) | $K^\sigma$ (nS) | $\Gamma_e$ (mol m$^{-2}$) | $\Gamma_n$ (mol m$^{-2}$) | $A_I$ (A$^2$) |
|---|---|---|---|---|---|
| $10^{-5}$ M KCl | −92.4 | 0.99 | $1.18\times10^{-8}$ | $1.20\times10^{-8}$ | 4,644 |
| $5\times10^{-5}$ M KCl | −85.4 | 1.29 | $2.18\times10^{-8}$ | $1.26\times10^{-8}$ | 3,526 |
| $10^{-4}$ M KCl | −76.8 | 1.43 | $2.59\times10^{-8}$ | $1.34\times10^{-8}$ | 3,156 |
| $10^{-5}$ M HCl | −63.2 | 1.22 | $0.60\times10^{-8}$ | $1.70\times10^{-8}$ | 4,156 |
| $10^{-5}$ M KOH | −145.8 | 1.66 | $3.30\times10^{-8}$ | $1.27\times10^{-8}$ | 2,839 |
| $5\times10^{-5}$ M KOH | −144.0 | 3.04 | $7.06\times10^{-8}$ | $1.81\times10^{-8}$ | 1,554 |
| $10^{-4}$ M KOH | −132.1 | 4.41 | $7.91\times10^{-8}$ | $3.93\times10^{-8}$ | 1,053 |

## 4.2 Grafted poly(L-glutamic acid) layer

In contrast to the case of the hydrophobic, molecularly smooth and chemically inert fluoropolymer layer grafted polypeptide chains exhibit rather dynamic interfacial structures towards aqueous electrolyte solution depending on the pH and electrolyte content of the adjacent solution.

The charge formation of the grafted poly (L-glutamic acid) layers was studied by streaming current measurements at varied pH in KCl solution concentration (Fig. 4). The position of the isoelectric point was determined at pH = 2.7 ± 0.1 indicating the presence of carboxylic acid groups at the surface to be the major charge formation process.

To quantify the accumulation of mobile charge carriers within the polypeptide layers, the surface conductivity

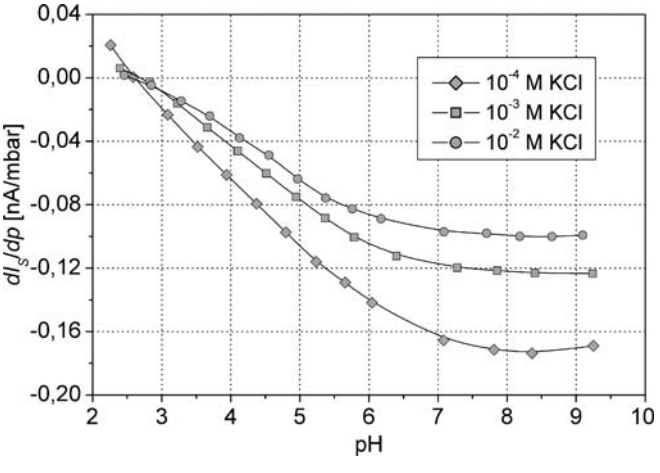


**Fig. 4** Streaming current versus pressure gradient in dependence of the solution pH for the grafted poly(L-glutamic acid) layers in $10^{-4}$, $10^{-3}$, and $10^{-2}$ M KCl solutions

was determined in $10^{-4}$, $10^{-3}$, and $10^{-2}$ M KCl solutions at pH = 6.0 and 9.0. As expected, the grafted polypeptide layers exhibit in general considerably higher values of the surface conductivity $K^{\sigma}$ (Table 2) when compared with the Teflon® AF films discussed above. This can be explained by the accumulation of mobile ions within the layer of grafted hydrophilic chains. The surface conductivity (which has in fact to be considered as a bulk conductivity of an interfacial nano-layer formed by the grafted ion penetrable polymers) was found to depend strongly on the pH and concentration of the solution (Table 2).

In the $10^{-4}$ M KCl solution, the ratio of $K^{\sigma}$ (pH = 9.0) to $K^{\sigma}$ (pH = 6.0) was determined to 35.1. For higher electrolyte concentrations, the corresponding values were 16.6 ($10^{-3}$ M KCl) and 5.2 ($10^{-2}$ M KCl), respectively. The increase in the surface conductivity at the different solution concentrations is also indicated by the Dukhin number versus pH plots (Fig. 5), which were obtained from streaming potential and streaming current data at channel heights of 50 μm. From the Du versus pH plots, it is obvious that the strongest increase of $K^{\sigma}$ occurs at about pH 8.3 in the $10^{-4}$ M and at about pH 7.5 in the $10^{-3}$ M KCl solution. Although the surface conductivity is increased with the electrolyte concentration, the Dukhin number vanishes to zero at the solution concentration of $10^{-2}$ mol $l^{-1}$. Therefore, the accumulation of mobile charge carriers in the polypeptide layer cannot be derived from the Du versus pH plot. However, the low ratio of $K^{\sigma}$ (pH = 9.0) to $K^{\sigma}$ (pH = 6.0) obtained for the $10^{-2}$ M KCl solution permits to conclude that $K^{\sigma}$ increases under these conditions at lower pH values as compared to the $10^{-4}$ and $10^{-3}$ M KCl solution.

The variation of the surface conductivity can be explained by charge-induced alterations of the structure of the poly(L-glutamic acid) chains. At low pH values, the polypeptide chains are uncharged and adopt an α-helical conformation (Paoletti et al. 1989). Consequently, a rather compact structure of the hydrodynamically immobile layer of the grafted polypeptide occurs. The low values of $K^{\sigma}$ at pH 6 indicate, that there is—in comparison to higher pH values—just a small amount of ions in the polypeptide layers sufficiently mobile to contribute to ion conduction. At high pH, the carboxyl side-groups, the grafted poly(L-glutamic acid) chains are negatively charged and—because of the electrostatic repulsion between the side-groups—their conformation is that of an extended coil (Paoletti et al. 1989). As a consequence, the thickness of the immobilized polypeptide layers is increased with increasing pH. The increase of the surface conductivity with increased pH can be ascribed to an increase of the total number of counter ions in the layer and to the less dense polymer network at the interface.

**Table 2** Experimentally determined surface conductivity for the surface grafted poly(L-glutamic acid) in $10^{-4}$, $10^{-3}$, and $10^{-2}$ M KCl solutions

| Solution | $K_{\sigma}$ (nS) |
|---|---|
| $10^{-4}$ M KCl, pH 6.0 | 4.5 |
| $10^{-4}$ M KCl, pH 9.0 | 157.9 |
| $10^{-3}$ M KCl, pH 6.0 | 10.6 |
| $10^{-3}$ M KCl, pH 9.0 | 179.6 |
| $10^{-2}$ M KCl, pH 6.0 | 40.6 |
| $10^{-2}$ M KCl, pH 9.0 | 209.9 |

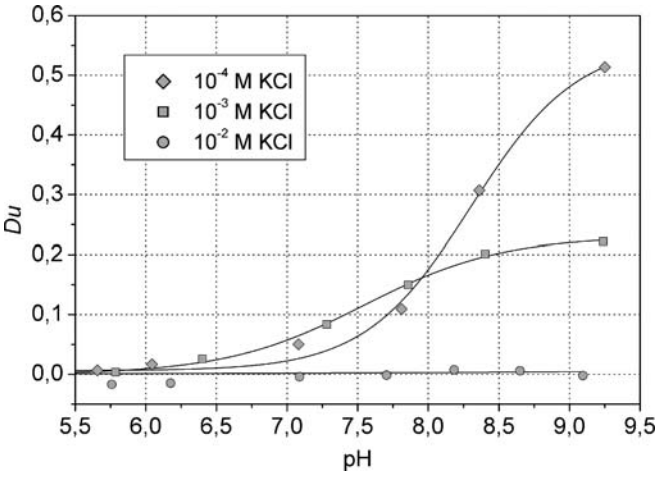


**Fig. 5** pH dependence of the Dukhin number Du (obtained from streaming potential and streaming current measurements at a channel height of 50 μm) for the poly(L-glutamic acid) layers in $10^{-4}$, $10^{-3}$, and $10^{-2}$ M KCl solutions

As discussed above, the surface conductivity increases at higher pH values in solutions of lower KCl concentration. This phenomenon can be explained by the increase of the apparent dissociation constant of the carboxylic acid groups with increased ionic strength of the electrolyte solution, i.e. the grafted poly(L-glutamic acid) chains behave more acidic at lower Debye screening radii (Nagasawa and Holtzer 1964; McDiarmid and Doty 1966). This finding further indicates that electrostatic interactions of acidic sites within the grafted chains inducing a p$K$-shift towards more acidic behaviour are most important for the conformational changes of the grafted polypeptide chains.

### 4.3 Self-assembled monolayers

The SAMs of alkenthiols on gold surfaces have widely been used for fundamental studies of surface forces in the past (Frisbie et al. 1994; Creager and Clarke 1994; van der Vegte and Hadziioannou 1997; Hu and Bard 1997; Kane and Mulvaney 1998; Kokkoli and Zukoski 2000). This is due to their unique property of a distinct surface chemistry and surface coverage of functional groups. The surface charge density ($\sigma_0$) of a SAM with COOH endgroups, therefore, is given by

$$\sigma_0 = -F\alpha\Gamma_m\chi^0_{COOH} \tag{15}$$

where $\Gamma_m$ is the surface coverage of the monolayer,

$\chi^0_{COOH}$, the surface fraction of COOH-terminated thiol, $F$, the Faraday constant and, $\alpha$, the degree of dissociation of the surface COOH groups, respectively. For a densely packed thiol SAM, $\Gamma_m$ is equal to $7.7\times10^{-10}$ mol cm$^{-2}$. The surface p$K$ value can be defined as

$$pK^0 = pH + \log\frac{[COO^-]^0}{[COOH]^0} = pH + \frac{\alpha}{1-\alpha}. \quad (16)$$

Combining the equations above and considering a Boltzmann distribution of protons near the interface

$$[H^+]_0 = 10^{-pH}\exp\left[-\frac{e\Psi_0}{k_B T}\right] \quad (17)$$

yields an expression which relates the surface potential ($\Psi_0$) to the p$K$ of the COOH groups (one-site dissociation model, see Kane and Mulvaney 1998; Kokkoli and Zukoski 2000; Healy and White 1978)

$$\sigma_0 = -\frac{F\Gamma_m\chi^0_{COOH}}{1 + pK^0 - pH + \frac{e\Psi_0}{2.303k_B T}}. \quad (18)$$

Using a variety of techniques, it has been found that the surface p$K$ in a self-assembled monolayer is substantially shifted to higher pH values due to strong in-plane electrostatic interactions (van der Vegte and Hadziioannou 1997; Hu and Bard 1997; Aoki and Kakiuchi 1999). These electrostatic interactions can either be lowered by a reduction of the surface density of COOH groups or by increasing the ionic strength. As revealed in Fig. 6, electrokinetic measurements using the MES confirm this concept.

With decreasing fraction of COOH groups in the SAM in binary systems, the isoelectric point decreases owing to the increased acidity of the remaining COOH groups (Schweiss et al. 2005). At very low fractions of COOH terminated thiols, it increases again as the unsymmetrical adsorption of ions onto the methyl-terminated sites becomes the prevailing charge formation process. The acidity is also affected by the polarity of the environment of the COOH groups as the shift to lower pH is more pronounced in the case of hydrophilic binary monolayer systems such as MUD/MUA. Accordingly, an increase of the ionic strength results in a lower isoelectric point as the in-plane electrostatic interactions between neighbouring COOH sites are effectively screened by the electrolyte counterions. Figure 6b shows a plot of the isoelectric point of a MHA SAM depending on the Debye parameter of the corresponding electrolyte.

Electrokinetic experiments on these binary SAM can additionally be used to evaluate the accuracy of the Gouy–Chapman theory. Equating the surface charge (Eq. 18) with the negative diffuse layer charge (Eq. 8), a Gouy–Chapman surface potential ($\Psi_{GC}$) can be calculated numerically. Figure 7 shows a comparison of the measured zeta potentials (from streaming current) for a pristine MHA SAM and abinary MUA/MUD-SAM (0.11/0.89) and the surface potentials obtained the GC approximation (solid lines). It is obvious that the Gouy–Chapman approximation is only valid for very low surface charge density such as the mixed SAM.

Unfortunately, the use of a gold substrate inhibits a thorough electrokinetic characterization including surface conductivity studies. This is because the underlying metal substrate provides an additional conduction path in the microchannel system and cannot be unambigously separated from the actual surface conductivity.

### 4.4 Poly(acrylic acid) brushes

The pH-dependent charging of the poly(acrylic acid) (PAA) layers was studied by streaming current experiments in $10^{-3}$ M KCl solutions. Since the swollen polymer chains themselves dissociate and create an ionized meshwork in part penetrated by the flowing solution, the determination of a discrete shear plane potential is certainly questionable and we restrict here on reporting and evaluating streaming current and surface conductivity data. The d$I_S$/d$p$ versus pH plot and the position of the isoelectric point at pH = 2.1 (Fig. 8) indicate that the surface charge originates from the dissociation of the carboxylic acid groups of the PAA chains. Above the isoelectric point (pH > 2.1), the mag-

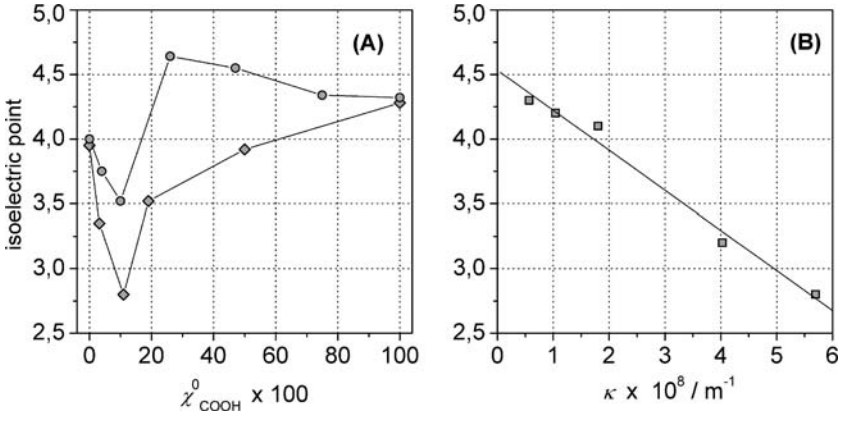


**Fig. 6** **a** Isoelectric point of mixed MUD/MUA (*diamond*) and MHA/HDT SAMs (*circle*) as a function of the surface fraction of COOH groups. **b** Isoelectric point of a MHA SAM versus the Debye parameter ($\kappa$) of the corresponding electrolyte solution

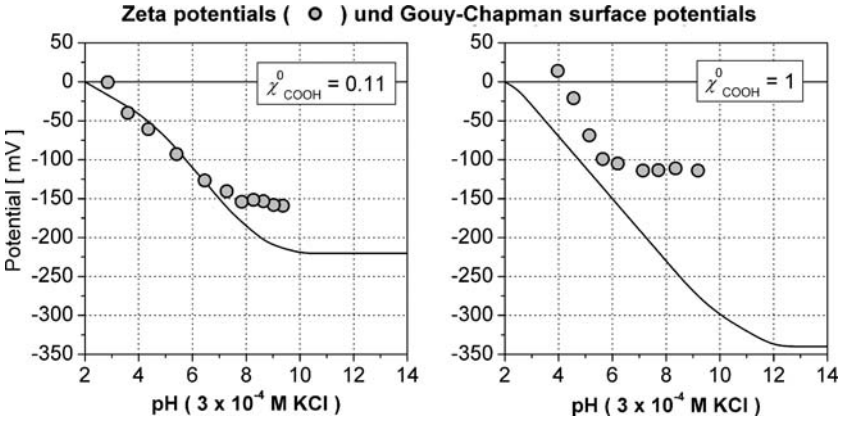


**Fig. 7** Comparison of the zeta potentials of a mixed SAM of MUA/MUD (0.11/0.89, left) and a MHA-SAM (right). The *solid lines* represent the corresponding Gouy–Chapman surface potentials ($\Psi_{GC}$) obtained from a one-site-binding model

nitude of the negative streaming current increases with the degree of deprotonation of the carboxylic acid groups at increasing pH values, until a plateau is reached in the basic region corresponding to full dissociation of the carboxylic acid.

To quantify the accumulation and distribution of mobile charge carriers at the interface, the surface conductivity was determined in a $10^{-3}$ M KCl solution at pH = 9.0. From $(dI_S/dp)/(dU_S/d_p)$ as a function of $h$ (Eq. 6) a value of 66.7 nS was obtained. As expected, the experimentally determined surface conductivity of the PAA brushes is very high at complete dissociation and must be due to the numerous counterions that are accumulated inside ($K^{\sigma,i}$) and outside ($K^{\sigma,d}$) of the brush.

The ion and potential distribution in the brush can be further analysed by a model developed by Ohshima (1995) and specified by Dukhin et al. (2004). According to this model, a polyelectrolyte layer is characterized by the Donnan potential $\Psi_D$, the potential value in the inner volume of the polyelectrolyte brush, and by the surface potential $\Psi_0$, attributed to the outermost edge of the polymer chains, respectively (Fig. 9). For the case of complete dissociation, $\Psi_D$ can be calculated from the fixed charge density in the layer and the electrolyte concentration of the adjacent solution:

$$\Psi_D = \frac{RT}{zF}\ \mathrm{asinh}\left(\frac{z_b s N}{2zcdN_A}\right), \tag{19}$$

where $R$ is the gas constant, $T$, the absolute temperature, $z$, the valence of the ions, $F$, the Faraday constant, $z_b$, the valence of the fixed charged groups, $s$, the number of

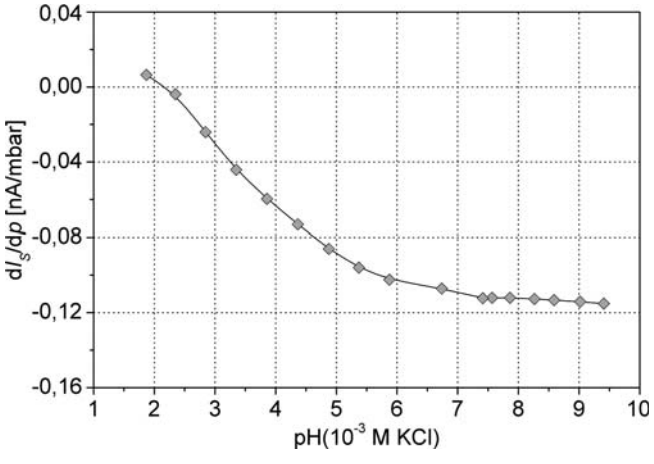


**Fig. 8** pH dependence of the streaming current versus pressure gradient ($dI_S/dp$) for the poly(acrylic acid) layer in a $10^{-3}$ M KCl solution

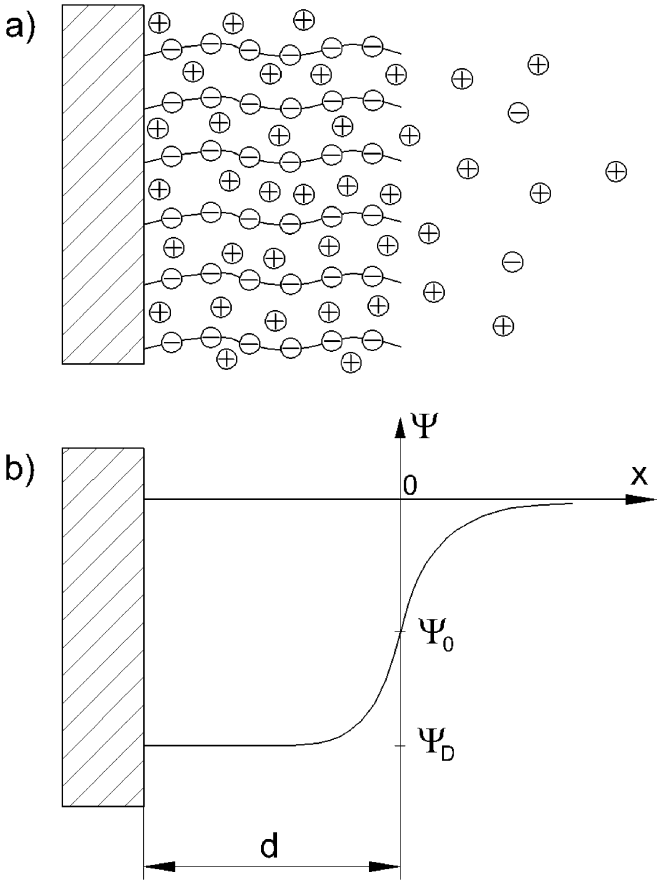


**Fig. 9** Ion Distribution (**a**) and potential distribution (**b**) near a surface covered with a negatively charged polyelectrolyte layer (Ohshima 1995)

grafted chains per meter squared, $N$, the number of charged groups per polymer chain, $c$, the solution concentration, $d$, the layer thickness, and, $N_A$, the Avogadro number. Subsequently, the surface potential $\Psi_0$ can be obtained using the following equation:

$$\Psi_0 = \Psi_D - \frac{RT}{zF}\tanh\left(\frac{zF\Psi_D}{2RT}\right). \quad (20)$$

With $N = 368$ and $d = 40$ nm, a Donnan potential of $-186$ mV and a surface potential of $-161$ mV were calculated for the brush in the case of complete dissociation.

The contribution of the diffuse layer charge "outside" the brush layer characterized by the potential $\Psi_0$—to the experimentally determined surface conductivity can be evaluated according to the Bikerman equation (9). Using this equation (9) and $\Psi_0 = -161$ mV, we obtain $K^{\sigma,d} = 4.6$ nS. In comparison with the experimentally determined surface conductivity of 66.7 nS this is about 7%, i.e. the vast majority of counterions is located within the brush. If we apply the classical Smoluchowski equation (3) for the evaluation of the streaming current data, a zeta potential of about $-60$ mV is obtained for pH = 9.0. This corresponds to less than 1% of the countercharge.

The well defined layer structure further permits to use the surface conductivity data to get an information about the ion mobility in the brush. If the ions outside the brush can move in an electrical field with the mobility $u_0$, the mobility $u$ of ions in the brush can be simply estimated from the charge distribution as follows:

$$u = \frac{K^{\sigma,i}}{esN - K_m^{\sigma,d}/u_0} \quad (21)$$

where $e$ is the elementary charge and $K_m^{\sigma,d}$ is the contribution of the diffuse layer to $K^{\sigma,d}$ caused by the movement of the ions with respect to the liquid (Dukhin et al. 2004). Assuming that for the case pH = 9, all 368 acrylic acid units in a chain are deprotonated, we find $u = 1.1\times10^{-8}$ m$^2$ V$^{-1}$ s$^{-1}$. This may be compared with the mobility of potassium ions in dilute electrolyte solution for which one has (from the tabulated equivalent conductance $\lambda$ of about 74 S cm$^2$ mol$^{-1}$) $u_0 = \lambda/F = 7.7\times10^{-8}$ m$^2$ V$^{-1}$ s$^{-1}$. Hence, the brush is very conductive, but the mobility of individual ions within the layer is not more than about 14% of their value in bulk electrolyte solution. The dramatically reduced ion mobility can be attributed to hydrodynamic, steric (tortuosity) effects and to electrostatic ion/brush interactions (Phillips 2000; Brinkman 1947; Johnson et al. 1996).

### 4.5 Adsorbed proteins at polymer thin films

The performance of biomedical technologies is often controlled by protein adsorption onto materials facing simple or complex biofluids. In view of the ubiquitous presence of protein adsorption, the process might be considered as a "translation" of surface properties of the solid towards any adjacent biosystem, in particular with regard to the fact that structural and functional alterations of adsorbed proteins are often sensed by cascade systems of living organisms. As the various interfacial "modes" of one given protein adsorbed at different material surfaces define important differences with respect to its functional features, the result of adsorption and desorption of FN (a key component of the extracellular matrix) at two negatively charged copolymer films with gradated hydrophobicity were presented in this section. The electrosurface characterization with the MES was complemented by the determination of the adsorbed mass (via optical thickness information by RIFS: reflectometric interference spectroscopy).

Thin films of alternating maleic acid copolymers containing either octadecene (POMA) or propene (PPMA) as comonomers provided acidic surfaces with varied hydrophobicity (and charge density). For the present work, substrates with advancing water contact angles of $(100 \pm 5)°$ for POMA and $(38 \pm 5)°$ for PPMA, respectively and similar isoelectric points of $1.9 \pm 0.1$ but different charge densities of 19 $\mu$C cm$^{-2}$ for POMA and 32 $\mu$C cm$^{-2}$ for PPMA were utilized (see Sect. 3). Differences in hydrophobicity and size of the comonomers determined the swelling behaviour of the films due to the balance between (attractive) hydrophobic and (repulsive) electrostatic interactions within and between the immobilized polymer chains. This was confirmed by surface conductivity data, reflecting the concentration of mobile ions at the interface: POMA showed significantly lower $K^\sigma$ values than PPMA (Table 3) and only the $K^\sigma$ data of PPMA were found to depend on the solution pH indicating that the degree of ionization of the maleic acid groups modulates the structure of the PPMA layers (Osaki and Werner 2003; Pompe et al. 2005).

The electrostatic and hydrophobic interactions determining the internal structure of the copolymer films clearly determine the adsorption behaviour of the proteins as well. This becomes obvious from the comparison of the adsorption dynamics of FN onto POMA and PPMA (Fig. 10): On the hydrophobic POMA, the characteristic pattern of a high-affinity adsorption was obtained showing a rapid coverage already at low solution concentrations of the protein and no desorption upon rinsing. In contrast, lower amounts of FN were adsorbed more slowly onto PPMA, gradually increasing with the protein solution concentration, and a certain fraction of the formed layer could be desorbed by rinsing with protein free solution. According to the electrokinetic measurements, the distinct differences in the electrosurface characteristics were also remarkably pronounced between the two. The weaker interaction between FN and PPMA showed a more acidic behaviour (lower IEP) of the FN-covered PPMA films (even at similar coverage) and a very different pattern of changes in $K^\sigma$ by FN adsorption (see Table 3).

**Table 3** Surface conductivity ($K^{\sigma}$) in $10^{-4}$ M KCl and isoelectric points (IEP) prior to and subsequent to FN adsorption at the copolymer thin films

| | POMA | | | PPMA | | |
|---|---|---|---|---|---|---|
| | $K^{\sigma}$ at pH 6 | $K^{\sigma}$at pH 9 | IEP | $K^{\sigma}$at pH 6 | $K^{\sigma}$at pH 9 | IEP |
| Polymer surface | 3.4 nS | 6.3 nS | 1.9 | 21.2 nS | 59.6 nS | 1.9 |
| With 50 μg ml$^{-1}$ FN | 4.4 | 10.7 | 4.2 | 7.1 | 17.4 | 2.9 |
| With 100 μg ml$^{-1}$ FN | 4.7 | 8.4 | 4.2 | 4.8 | 23.0 | 3.2 |
| With 200 μg ml$^{-1}$ FN | | | | 6.7 | 24.0 | 3.2 |

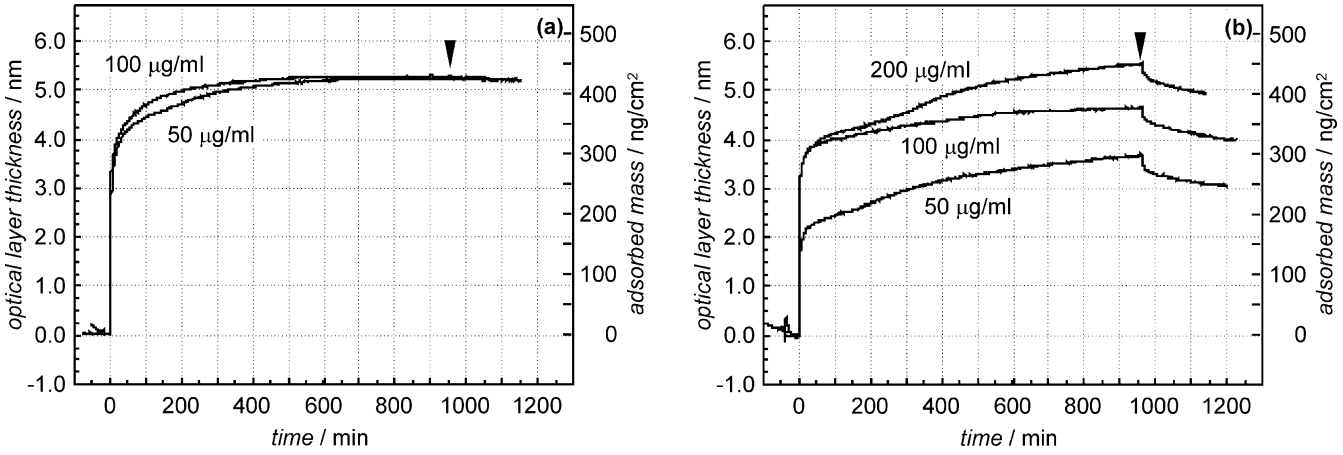


**Fig. 10** Three Dynamics of FN adsorptions onto POMA (**a**) and PPMA (**b**) was followed in situ by RIfS at FN solution concentration from 50 to 200 μg ml$^{-1}$ (desorption was done by rinsing with pure PBS at the *arrows*). The measured optical thicknesses of FN layers were also translated into the adsorbed protein mass using de Feijter's equation (de Feither et al. 1978; Vorös 2004). The results correlate well with previous own data based on amino acid analysis with HPLC (Renner et al. 2005). The electrokinetic experiments shown in Table 3 were performed before and after the adsorptions without de-wetting the surfaces

The IEP of FN-coated POMA (pH 4.2) approached the intrinsic value of the protein (at about pH 5, Toony et al. 1983) pointing at a rather stochastic orientation of FN on POMA without neither electrostatic matching with the substrate nor dramatic structural changes of the protein. In contrast, the FN adsorption/desorption characteristics on PPMA (Fig. 10) was accompanied by a significantly lower IEP of the resulting FN layers. In view of these findings and the absence of strong hydrophobic interactions, we concluded on electrostatically driven FN adsorption, i.e. the attachment of the protein due to attraction between positively charged residues of the protein and the negatively charged polymer functional groups, resulting in a charge orientation of the protein in the interfacial layer (Wilson et al. 2004). Both the more acidic IEP of the protein layer and the decrease of $K^{\sigma}$ during the FN adsorption onto PPMA impressively support the idea of an electrostatically controlled adsorption. This conclusion is also in line with the conclusions drawn from a recent own quartz crystal microbalance study (Vörös 2004; Renner et al. 2004).

The elaborated example clearly shows that different modes of a given protein can be obtained at interfaces depending on the kind of solid substrate—and conveniently detected with the help of the MES-RIfS combination. In consequence, the availability of the adsorbed protein for secondary binding, conformational changes and displacement can be expected to exhibit differences as well. Along that line, the compared interfacial modes of FN on the copolymer substrates used in this set of experiments were further shown to trigger the reorganization of the immobilized protein by adherent endothelial cells into supramolecular assemblies (Pompe et al. 2005), and, in turn, switch cellular fate decisions of the adherent cells from proliferation to angiogenesis (Pompe et al. 2004).

## 5 Conclusions and perspective

By means of the MES, the simultaneous determination of zeta potential $\zeta$ and surface conductivity $K^{\sigma}$ of planar solid/liquid interfaces can be realized since streaming potential and streaming current measurements are evaluated to obtain these data. The application of macroscopic planar surfaces (20×10 mm$^2$) as sample materials permits to study a wide variety of very different interfacial phenomena by this type of experiment. For any of the analysed examples, the tangentially mobile charge at the solid/liquid interface is dominated by charge carriers located in the hydrodynamically stagnant layer behind the shear plane. A more detailed

interpretation of the charge carrier distribution and mobility has to be based on structural information about the interface for any solution characteristics considered. With regard to this, the combination of the surface conductivity measurements with the simultaneous determination of optical and hydrodynamic layer thickness of the analysed samples is highly desirable. Ongoing activities of the authors address that need. In addition, the demonstrated experimental progress in the characterization of planar solid/liquid interfaces asks for the development of a more advanced theory of electrosurface phenomena treating both the structure of the electrical double layer and the charge formation process.

## References


Aoki K, Kakiuchi T (1999) p*Ka* of an $\omega$-carboxylalkanethiol self-assembled monolayer by interaction model. J Electroanal Chem 478:101–107

Baerga-Ortiz A, Rezaie AR, Komives EA (2000) Electrostatic dependence of the thrombin–thrombomodulin interaction. J Mol Biol 296:651–658

Bikerman JJ (1935) Die Oberflächenleitfähigkeit und ihre Bedeutung. Kolloid Z 72:100–108

Bismarck A, Kumru ME, Springer J (1999) Characterization of several polymer surfaces by streaming potential and wetting measurements: some reflections on acid–base interactions. J Colloid Interface Sci 217:377–387

Brew SA, Ingham KC (1994) Purification of human plasma fibronectin. J Tissue Cult Methods 16:197–199

Brinkman HC (1947) A calculation of the viscous force exerted by a flowing fluid on a dense swarm of particles. Appl Sci Res A1:27–34

Creager SE, Clarke JE (1994) Contact-angle titrations of mixed omega—mercaptoalkanoic acid/alkanethiol monolayers on gold. Reactive versus nonreactive spreading, and chain length effects on surface p*Ka* values. Langmuir 10:3675–3683

Currie EPK, Leermakers FAM, Cohen Stuart MA, Fleer GJ (1999a) Grafted adsorbing polymers: scaling behavior and phase transitions. Macromolecules 32:487–498

Currie EPK, Sieval AB, Avena M, Zuilhof H, Sudhölter EJR, Cohen Stuart MA (1999b) Weak polyacid brushes: preparation by LB deposition and optically detected titrations. Langmuir 15:7116–7118

Currie EPK, van der Gucht J, Borisov OV, Cohen Stuart MA (1999c) Stuffed brushes: theory and experiment. Pure Appl Chem 71:1227–1241

Currie EPK, Wagemaker M, Cohen Stuart MA, van Well AA (1999d) Structure of monodisperse and bimodal brushes. Macromolecules 32:9041–9050

Currie EPK, Sieval AB, Fleer GJ, Cohen Stuart MA (2000) Polyacrylic acid brushes: surface pressure and salt-induced swelling. Langmuir 16:8324–8333

Dukhin SS, Derjaguin BV (1974) Electrokinetic phenomena. In: Matijevic E (ed) Surface and colloid science, vol 7. Wiley, New York

Dukhin SS, Zimmermann R, Werner C (2004) Intrinsic charge and Donnan potentials of grafted polyelectrolyte layers determined by surface conductivity data. J Colloid Interface Sci 274:309–318

Dukhin SS, Zimmermann R, Werner C (2005) Electrokinetic phenomena at grafted polyelectrolyte layers. J Collid Interface Sci 286:761–773

Duval JFL, van Leeuwen HP (2004) Electrokinetics of diffuse soft interfaces. 1. Limit of low potentials. Langmuir 20:10324–10336

Erickson D, Li D (2002) Microchannel flow with patchwise and periodic surface heterogeneity. Langmuir 18:8949–8959

de Feijter JA, Benjamins J, Veer FA (1978) Ellipsometry as a tool to study the adsorption behavior of synthetic and biopolymers at the air–water interface. Biopolym 17:1759–1772

Fodor SPA, Rava RP, Huang XC, Pease AC, Holmes CP, Adams CL (1993) Multiplexed biochemical assays with biological chips. Nature 364:555–556

Frisbie CD, Rozsnyai LF, Noy A, Wrighton MS, Lieber CM (1994) Functional group imaging by chemical force microscopy. Science 265:2071–2074

Garbassi F, Morra M, Occhiello E (1996) Polymer surfaces: from physics to technology. Wiley, Chichester

Grundke K, Jacobasch HJ, Simon F, Schneider S (1995) Physicochemical properties of surface-modified polymers. J Adhes Sci Technol 9:327–350

Healy TW, White LR (1978) Ionizable surface group models of aqueous interfaces. Adv Colloid Interface Sci 9:303–345

Hu K, Bard AJ (1997) Use of atomic force microscopy for the study of surface acid–base properties of carboxylic acid-terminated self-assembled monolayers. Langmuir 13:5114–5119

Hunter RJ (1981) Zeta potential in colloid science: principles and applications. Academic, London

Jacobasch HJ (1984) Oberflächenchemie faserbildender Polymerer. Akademie Verlag, Berlin

Jacobasch HJ, Schurz J (1988) Characterization of polymer surfaces by means of electrokinetic measurements. Progr Colloid Polym Sci 77:40–48

Jeon SI, Andrade JD (1991) Protein–surface interactions in the presence of polyethylene oxide. J Colloid Interface Sci 142:159–166

Johnson EM, Berk DA, Jain RK, Deen WM (1996) Hindered diffusion in agarose gels: test of effective medium model. Biophys J 70:1017–1023

Kane V, Mulvaney P (1998) Double-layer interactions between self-assembled monolayers of mercaptoundecanoic acid on gold surfaces. Langmuir 14:3303–3311

Kokkoli E, Zukoski CF (2000) Surface forces between hydrophilic self-assembled monolayers in aqueous electrolytes. Langmuir 16:6029–6036

Körber H, Werner C, Jacobasch HJ (1999) Micro-slit cell. Patent WO 99/30141

Liu X, Farmerie W, Schuster S, Tan W (2000) Molecular beacons for DNA biosensors with micrometer to submicrometer dimensions. Anal Biochem 283:56–63

Löbbus M, van Leeuwen HP, Lyklema J (2000) Streaming potentials and conductivities of latex plugs. Influence of the valency of the counterion. Colloids Surf A 61:103–113

Lyklema J (1995) Fundamentals of colloid and interface science, vol 2, solid–liquid interfaces, Academic, London

Lyklema J, Rovillard S, Coninck JD (1998) Electrokinetics: the properties of the stagnant layer. Langmuir 14:5659–5663

McDiarmid R, Doty P (1966) The spectrophotometric titration of polyacrylic, poly-L-aspartic, and poly-L-glutamic acids. J Phys Chem 70:2620–2627

Minor M, van der Linde AJ, Lyklema J (1998) Streaming potentials and conductivities of latex plugs in indifferent electrolytes. J Colloid Interface Sci 203:177–188

Nagasawa M, Holtzer A (1964) The helix–coil transition in solutions of polyglutamic acid. J Am Chem Soc 86:538–543

Nitzsche R, Simon F (1997) Bestimmung des Zetapotentials aus Messungen der elektrophoretischen Mobilität. Technisches Messen 64:106–113

Ohshima H (1995) Electrophoretic mobility of soft particles. Colloids Surf A 103:249–255

Osaki T, Werner C (2003) Ionization characteristics and structural transitions of alternating maleic acid copolymer films. Langmuir 19:5787–5793

Paoletti S, Cesaro A, Samper CA, Benegas JC (1989) Conformational transitions of poly($\alpha$-L-glutamic acid). A polyelectrolytic approach. Biophys Chem 34:301–309

Phillips RJ (2000) A hydrodynamic model for hindered diffusion of proteins and micelles in hydrogels. Biophys J 79:3350–3354

Pompe T, Zschoche S, Salchert K, Herold N, Gouzy MF, Sperling C, Werner C (2003) Maleic anhydride copolymers—a versatile platform for molecular biosurface engineering. Biomacromolecules 4:1072–1079

Pompe T, Markowski M, Werner C (2004) Modulated fibronectin anchorage at polymer substrates controls angiogenesis. Tissue Eng 10:841–848

Pompe T, Renner L, Grimmer M, Herold N, Werner C (2005) Functional films of maleic anhydride copolymers under physiological conditions. Macromol Biosci 5:890–895

Pompe T, Renner L, Werner C (2005) Nanoscale features of fibronectin fibrillogenesis depend on protein–substrate interaction and cytoskeleton structure. Biophys J 88:527–534

van der Put AG (1980) Electrokinetic investigations on the system polystyrene/aqueous electrolyte solution. PhD thesis, Wageningen Agricultural University

Renner L, Pompe T, Salchert K, Werner C (2004) Dynamic alterations of fibronectin layers on copolymer substrates with graded physicochemical characteristics. Langmuir 20:2928–2933

Renner L, Pompe T, Salchert K, Werner C (2005) Fibronectin displacement at polymer surfaces. Langmuir 21:4571–4577

Riepl M, Mirsky VM, Novotny I, Tvarozek V, Rehacek V, Wolfbeis OS (1999) Optimization of capacitive affinity sensors: drift suppression and signal amplification. Anal Chim Acta 392:77–84

Schmitt FJ (2002) Wechselwirkungen und Adhäsion von Polymer-Grenzflächen. Habilitation thesis, Dresden University of Technology

Schweiss R, Pleul D, Simon F, Janke A, Welzel PB, Voit B, Knoll W, Werner C (2004) Electrokinetic potentials of binary self-assembled monolayers on gold: acid–base reactions and double layer struture. J Phys Chem B 108:2910–2917

Schweiss R, Welzel P, Knoll W, Werner C (2005) Assembly modulates dissociation: electrokinetic experiments reveal peculiarities of the charge formation at monolayer films. Chem Comm 256–258

Stroock AD, Weck M, Chiu DT, Huck WTS, Kenis PJA, Ismagilov RF, Whitesides GM (2000) Patterning electroosmotic flow with patterned surface charge. Phys Rev Lett 84:3314–3317

Toony NM, Mosesson MW, Amrani DL, Hainfeld JF, Wall JS (1983) Solutions and surface effects on plasma fibronectin structure. J Cell Biol 97:1686–1692

Uyama Y, Kato K, Ikada Y (1998) Surface modification of polymers by grafting. Adv Polym Sci 137:1–39

van der Vegte EW, Hadziioannou G (1997) Acid–base properties and the chemical imaging of surface-bound functional groups studied with scanning force microscopy. J Phys Chem B 101:9563–9569

Vörös J (2004) The density and refractive index of adsorbing protein layers. Biophys J 87:553–561

van Wagenen RA, Andrade JD (1980) Flat plate streaming potential investigations: hydrodynamics and electrokinetic equivalency. J Colloid Interface Sci 76:305–314

Werner C, Körber H, Zimmermann R, Dukhin SS, Jacobasch HJ (1998) Extended electrokinetic characterization of flat solid surfaces. J Colloid Interf Sci 208:329–346

Werner C, König U, Augsburg A, Arnhold C, Körber H, Zimmermann R, Jacobasch HJ (1999) Electrokinetic surface characterization of biomedical polymers—a survey. Colloids Surf A 159:519–529

Wilson K, Stuart SJ, Garcia AJ, Latour RA (2004) A molecular modeling study of the effect of surface chemistry on the adsorption of a fibronectin fragment spanning the 7–10th type III repeats. J Biomed Mater Res 69A:686–698

Yezek LP (2005) Bulk conductivity of soft surface layers: experimental measurement and electrokinetic implications. Langmuir 21:10054–10060

Zimmermann R, Dukhin SS, Werner C (2001) Electrokinetic measurements reveal interfacial charge at polymer films caused by simple electrolyte ions. J Phys Chem B 105:8544–8549

Zimmermann R, Birkert O, Gauglitz G, Werner C (2003) Electrosurface Phenomena at Polymer Films for Biosensor Applications. Chem Phys Chem 4:509–514